SIAM J. APPL. MATH.
Vol. 72, No. 1, pp. 240–260

NONLINEAR WAVES IN SHALLOW HONEYCOMB LATTICES*

MARK J. ABLOWITZ† AND YI ZHU‡

Abstract. The linear spectrum and corresponding Bloch modes of shallow honeycomb lattices near Dirac points are investigated. Via perturbation theory, the dispersion relation is found to have threefold degeneracy at leading order with eigenvalue splitting at the following two orders; i.e., the threefold eigenvalue splits into single and double values. Multiscale perturbation methods are employed to describe the nonlinear dynamics of the associated wave envelopes. The dynamics of the envelope depends on different asymptotic balances whereupon a three-level nonlinear Dirac-type equation or a two-level nonlinear Dirac equation is derived. The analysis agrees well with direct numerical simulations.

Key words. honeycomb lattices, nonlinear Dirac equation, coupled mode equation

AMS subject classifications. 41A60, 35C20, 35Q55, 35L60

DOI. 10.1137/11082662X

1. Introduction.

Two-dimensional honeycomb (HC) lattices have attracted considerable interest in both physics and applied mathematics, stimulated in part by the recent fabrication of the material graphene [1, 2], which itself has atoms arranged in an HC lattice structure. This special structure also arises in the Bose–Einstein condensation (BEC) [3, 4] and nonlinear optical beam propagation in photonic crystals [5, 6, 7, 8].

Interestingly, a central equation in all of the above applications is the lattice nonlinear Schrödinger (NLS) equation, which is given in dimensionless form as

$$i\partial_z\psi + \Delta\psi - \delta V(\mathbf{r})\psi + \sigma|\psi|^2\psi = 0, \tag{1.1}$$

where $\mathbf{r} = (x, y) \in \mathbb{R}^2$, $V(\mathbf{r})$ is a real-valued, periodic, and smooth function, $\delta > 0$, and σ are constants. For the local and global well-posedness of the initial value problem with arbitrary initial conditions, see, for example, [9, 10].

In graphene, the nonlinear effect is negligible, i.e., $\sigma = 0$; here (1.1) describes the dynamics of the quantum states of the electrons. In nonlinear optics, this equation describes electromagnetic waves propagating in inhomogeneous, Kerr nonlinear media. The equation can be derived from the Maxwell equations by assuming a unidirectionally polarized field and the paraxial approximation (see, e.g., [11, 12]); here z is the propagation direction, $V(\mathbf{r})$ represents the spatial variation of the linear refractive index, and σ is the nonlinear coefficient which is positive for focusing or negative for defocusing nonlinearity. In BECs, the above NLS equation is often called the Gross–Pitaevskii (GP) equation. In this context, it describes the dynamics of a macroscopic quantum state of ultracold atoms being trapped in an optical lattice in

*Received by the editors March 7, 2011; accepted for publication (in revised form) November 14, 2011; published electronically January 26, 2012. This research was partially supported by the U.S. Air Force Office of Scientific Research under grant FA9550-09-1-0250 and by the NSF under grant DMS-0905779.

http://www.siam.org/journals/siap/72-1/82662.html

†Department of Applied Mathematics, University of Colorado, 526 UCB, Boulder, CO 80309-0526 (mark.ablowitz@colorado.edu).

‡Corresponding author. Zhou Pei-Yuan Center for Applied Mathematics, Tsinghua University, Beijing 100084, China (yizhu@tsinghua.edu.cn).

the mean-field limit. The nonlinearity is due to two-particle interactions, and the nonlinear coefficient σ corresponds to the scattering length (see, e.g., [13, 14]).

Whereas in graphene the dynamics of quantum states are linear, in optics or BECs nonlinearity often plays a significant role. In HC lattice investigations of photonics, researchers have used the term photonic graphene. The resulting wave propagation in HC photonic lattices has led to interesting and novel phenomena *which has not been found in other lattices.* Examples include, but are not limited to, two-dimensional gas of fermions and corresponding dynamics [1, 2, 3], conical diffraction [6, 7], broken time-reversal symmetry [8], etc. Hence it is important to develop a fundamental understanding of the wave dynamics, both linear and nonlinear, in HC lattices.

A linear eigenvalue problem naturally associated with (1.1) is obtained by taking $\sigma = 0$ and $\psi(z, \mathbf{r}) = \varphi(\mathbf{r})e^{-i\mu z}$. Namely, we are led to the Schrödinger eigenvalue problem

$$\mathcal{H}\varphi = (-\Delta + \delta V(\mathbf{r}))\varphi = \mu\varphi,$$

where $\mu \in \mathbb{R}$ is the eigenvalue and $\varphi(\mathbf{r})$ is the corresponding eigenfunction. From Bloch–Floquet theory [15], the eigenfunction has the form $\varphi(\mathbf{r}) = e^{i\mathbf{k}\cdot\mathbf{r}}U(\mathbf{r};\mathbf{k})$, where $U(\mathbf{r};\mathbf{k})$ has the same periodicity as the potential $V(\mathbf{r})$; $\mathbf{k}$ is termed the Bloch wave vector and $\mu(\mathbf{k})$ in terms of $\mathbf{k}$ is called the dispersion relation. For a fixed $\mathbf{k}$, $\mu(\mathbf{k})$ usually has infinitely many values, denoted as $\mu^{(n)}(\mathbf{k})$, $n \geq 1$; $\mu^{(n)}(\mathbf{k})$ is called the nth band of the dispersion relation. Between two nearby bands there can exist an interval where a real-valued dispersion relation (or eigenvalue) $\mu(\mathbf{k})$ does not exist; this interval is called a *band gap.* Further details are included in section 2.

In general position the wave dynamics associated with the 2+1-dimensional NLS equation (1.1) is complex. Without nonlinearity ($\sigma = 0$), an initial condition can be decomposed into Bloch components due to the completeness of Bloch modes in $L^2(\mathbb{R}^2)$ [16]. The superposition principle ensures that each component propagates on its own following the dispersion relation [15]. However, in the nonlinear case ($\sigma \neq 0$), the superposition principle no longer holds and different Bloch components influence each other due to nonlinear interactions. In many applications the dynamics of the wave packets associated with one or several Bloch modes, where the envelope scale is much longer than the lattice scale, are of central interest. The asymptotic method of multiple scales is useful and leads to envelope equations on a slow evolution scale. In order to study such phenomena the original 2+1-dimensional governing equation (1.1) is computationally difficult due to the large ratio between the envelope and lattice scales; furthermore inserting the fine lattice scale is unwieldy. In addition the governing equation does not indicate the key physical and mathematical basis of the underlying envelopes. Hence in order to understand the macroscopic dynamics, it is important to understand Bloch theory and derive homogenized equations by averaging out the lattice scale.

Recently, considerable progress has been made in developing homogenized equations associated with the lattice NLS equation (1.1) in the case of simple lattices (having a basis of one minima per unit cell). Generally speaking, as long as the dispersion relation $\mu(\mathbf{k})$ is analytic in the neighborhood of a point $\mathbf{k}_0$ and we consider a single envelope, the resulting envelope equation is the scalar NLS equation where $\nabla\mu(\mathbf{k}_0)$ is the group velocity and next order dispersion is determined by the second derivatives of $\mu(\mathbf{k_0})$ [17, 18]. Similarly if the initial input contains more than one envelop, the dynamics can be governed by nonlinear coupled mode equations [19, 20, 21, 22, 23]. There can also be degenerate cases where two adjacent bands intersect each other at

a point, $\mathbf{k}_0$. For instance if $\mu^{(n)}(\mathbf{k}_0) = \mu^{(n+1)}(\mathbf{k}_0)$, coupled NLS-type equations can be derived so long as each band is analytic in the neighborhood of $\mathbf{k}_0$ [18]. In terms of solutions of the effective NLS-type equations, localized pulses, i.e., solitons, can exist in band gaps. They are usually called gap solitons (nonlinear localized modes lying in the band gaps). Gap solitons associated with both simple and coupled NLS-type equations have been investigated [24, 25, 26, 27].

However, HC lattices have some special features, which we mention below, that distinguish themselves from any of the above cases. An HC lattice is a two-dimensional periodic lattice whose minima are arranged in a hexagonal structure as shown in Figure 2.1(b). It can be seen as a hexagonal lattice with a basis of two minima per unit cell. Physically speaking, a honeycomb lattice can be generated by interfering three plane waves [6],

$$V(\mathbf{r}) = \left|e^{ik_0\mathbf{b}_1\cdot\mathbf{r}} + e^{ik_0\mathbf{b}_2\cdot\mathbf{r}} + e^{ik_0\mathbf{b}_3\cdot\mathbf{r}}\right|^2 - 3, \tag{1.2}$$

where $\mathbf{b}_1 = (0,1)$, $\mathbf{b}_2 = (-\frac{\sqrt{3}}{2}, -\frac{1}{2})$, and $\mathbf{b}_3 = (\frac{\sqrt{3}}{2}, -\frac{1}{2})$ and k_0 is a constant (typical lattice wave number). A special feature of HC lattices is that the lowest two bands touch each other at distinct points ($\mathbf{K}$ and $\mathbf{K}'$ in Figure 2.1(c)). This is different from a typical band intersection. These isolated touching points of the two-dimensional dispersion surface are usually called Dirac points. In the vicinity of these Dirac points, the dispersion relation is not analytic at these points; it has a conical structure (see, e.g., Figure 3.1(a)). This nonanalytic behavior in the dispersion relation leads to the major differences from the above studies. Physically speaking, the conical nature of the dispersion relation at the Dirac points gives rise to the existence of massless Dirac fermions in graphene [1, 2] and conical wave diffraction in photonics applications [6, 7, 28, 29]. In some applications, nonlinearity can be very important, which in turn gives rise to markedly different dynamics from the linear case. This further motivates the study of the nonlinear dynamics associated with the Dirac points.

In (1.1), if $\delta \gg 1$, the potential $V(\mathbf{r})$ has very deep wells at their minima. The associated study, called the tight-binding limit, leads to analytical results for both Bloch theory [30] and nonlinear wave dynamics [31, 32] where novel discrete systems and their continuum limits are obtained. In the latter case, the wave envelopes associated with points which are *not* near the Dirac points are governed by effective NLS equations. However, in the vicinity of Dirac points, the envelope equations are governed by Dirac equations, which in turn leads to conical wave diffraction which agrees with experiment observations [31, 32].

On the other hand, the shallow HC potential limit, i.e., $\delta \ll 1$, is also an important limit to consider in photonic crystals and BECs. To date there are very few results on the HC lattices in this limit, the persistence of Dirac points and corresponding wave dynamics. The only aspects studied to date involve the linear problem [8]. The slowly varying nonlinear wave envelope equations and associated asymptotic analysis in the neighborhood of the Dirac points for the shallow lattice problem discussed in this paper are new. The nonlinear envelope system allows one to readily study the behavior of a Dirac wave packet; this is difficult to do within the framework of the original NLS equation since large-scale variations and all Bloch components are contained. These envelope equations allow one to study, for example, the nonlinear effects associated with the wave dynamics and the diffraction wave patterns, both of which can potentially be observed in experiment. In simple lattices such wave diffraction patterns are not found.

The paper is organized as follows. In section 2 the HC potential and the essentials of the Bloch theory for the linear Schrödinger equation with a periodic potential, which will be needed in what follows, are given. Section 3 focuses on the lowest Bloch mode band and outlines the perturbation results at a Dirac point. These points have special properties. There are three modes. The dispersion curves as a function of potential strength, assumed small here, are developed for the lowest bands. At leading order the dispersion curve has a triple root at special points called Dirac points. At the next two subsequent orders the triple root separates into two double and one simple root. Indeed we find this to hold perturbatively at many subsequent orders. Similarly when we have a strong lattice potential, (i.e., in the tight-binding limit [30]), the dispersion relation is degenerate at these special points. We conjecture that there is indeed a degeneracy for arbitrary δ. In section 4 the envelope associated with the Bloch modes are shown to satisfy nonlinear wave equations of Dirac type. There are different equations depending on the assumed maximal balance between weak nonlinearity and the slow evolution of the envelope and how this slowness depends on the shallowness of the potential. We note that even when there is no spatial variation, the ("Landau"-type) equations are not trivial. We investigate two balances. In the faster evolution we find a third order evolution system. Corresponding to typical initial conditions we find that this system evolves into a triangular structure. In the slower evolution case, the equations decouple into a coupled second order system and a third single equation. The coupled second order system is a nonlinear Dirac system which possesses conical diffraction, with and without a "notch." Conical diffraction was found experimentally and computationally in [6]. A discrete and continuous nonlinear Dirac system was derived in the strong potential (tight-binding) limit and shown to possess conical diffraction in the neighborhood of a Dirac point; discrete and continuous NLS-type equations were derived away from Dirac points [31, 32].

2. Preliminaries. We consider the Schrödinger operator $\mathcal{H} = -\Delta + V(\mathbf{r})$ acting in $L^2(\mathbb{R}^2)$ in the sense of Hilbertian integrals [15], where $V(\mathbf{r})$ is a smooth, real-valued, periodic potential. We denote $\mathbf{v}_1$ and $\mathbf{v}_2$ as the two primitive lattice vectors. The set

$$\Omega = \left\{ \sum_{j=1}^{2} q_j \mathbf{v}_j : q_j \in [0,1] \right\}$$

is the primitive unit cell. In the dual spectral space, the primitive reciprocal lattice vectors $\mathbf{k}_1$ and $\mathbf{k}_2$ satisfy $\mathbf{v}_i \cdot \mathbf{k}_j = 2\pi\delta_{ij}$, where δ_{ij} is the Kronecker delta function. Similarly the primitive reciprocal unit cell, i.e., the Brillouin zone, is defined by

$$\Omega' = \left\{ \sum_{j=1}^{2} q_j \mathbf{k}_j : q_j \in \left[-\frac{1}{2}, \frac{1}{2} \right] \right\}.$$

The characteristic vectors of the HC lattice (1.2) are

$$\mathbf{v}_1 = \frac{4\pi}{3k_0}\left(\frac{\sqrt{3}}{2}, \frac{1}{2}\right), \qquad \mathbf{v}_2 = \frac{4\pi}{3k_0}\left(\frac{\sqrt{3}}{2}, -\frac{1}{2}\right),$$
$$\mathbf{k}_1 = \sqrt{3}k_0\left(\frac{1}{2}, \frac{\sqrt{3}}{2}\right), \qquad \mathbf{k}_2 = \sqrt{3}k_0\left(\frac{1}{2}, -\frac{\sqrt{3}}{2}\right).$$

It is useful to note that the potential can be written as

$$V(\mathbf{r}) = e^{i\mathbf{k}_1\cdot\mathbf{r}} + e^{i\mathbf{k}_2\cdot\mathbf{r}} + e^{i(\mathbf{k}_1+\mathbf{k}_2)\cdot\mathbf{r}} + c.c.,$$

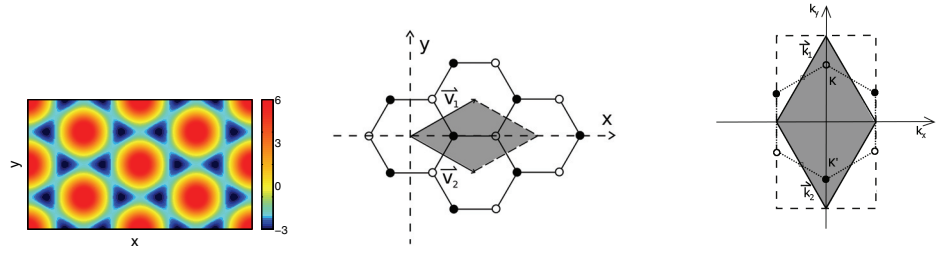

(a) (b) (c)

FIG. 2.1. *The HC potential* (a)*, the connection of local minima* (b)*, and its Brillouin zone* (c)*. The dots and circles are the positions of local minima. The shaded regions in* (b) *and* (c) *are the primitive unit cell and the Brillouin zone, respectively.*

where *c.c.* represents the complex conjugate.

An HC lattice is a special two-dimensional lattice whose local minima (called sites) are arranged in a hexagonal structure. The construction of the HC lattice and its Brillouin zone is shown in Figure 2.1. There are two sites per unit cell. We remark that the above primitive and reciprocal unit cells are parallelograms generated by $\mathbf{v}_1$, $\mathbf{v}_2$, and $\mathbf{k}_1$, $\mathbf{k}_2$ respectively. However, in the literature hexagonal tiles (Wigner–Seitz cells) are often used as the unit cells in the physical and reciprocal lattices [33]. The two representations, parallelograms and hexagons, are essentially the same due to the periodicity. For example, in Figure 2.1(b) the shaded region and the hexagon surrounded by the dotted line are both equivalent representations of the unit cell.

It is also noted that equilateral triangular lattices, sometimes referred to as hexagonal lattices, and HC lattices have the same periodicity. In the tight-binding limit, the difference is essential. Triangular lattices have only one minimum per cell and as such they are simple lattices; on the other hand, HC lattices have two minima per cell. In the shallow potential case, the lowest bands of dispersion relation in different lattices are completely different. The lowest eigenvalue of HC lattices at Dirac points is degenerate (see below), while the lowest eigenvalue of triangle lattices is simple [34].

According to Floquet–Bloch theory (see, for example, [16, 15]), the eigenfunction, referred as a *Bloch mode*, of the Schrödinger operator $\mathcal{H}$ is of the form

$$\varphi(\mathbf{r}, \mathbf{k}) = e^{i\mathbf{k}\cdot\mathbf{r}} U(\mathbf{r}; \mathbf{k}),$$

where $\mathbf{k} \in \Omega'$ is the Bloch wave vector (often called the quasi-momentum) and $U(\mathbf{r}; \mathbf{k})$ for any $\mathbf{k} \in \Omega'$ has the same periodicity as $V(\mathbf{r})$. The real-valued eigenvalue $\mu(\mathbf{k})$ as a function of $\mathbf{k}$ is usually called the dispersion relation of the potential $V(\mathbf{r})$. For each $\mathbf{k} \in \Omega'$, we have the following eigenvalue problem in $L^2_{per}(\Omega)$:

$$\begin{aligned} \mathcal{H}_{\mathbf{k}} U(\mathbf{r}; \mathbf{k}) &= \mu(\mathbf{k}) U(\mathbf{r}; \mathbf{k}), \\ U(\mathbf{r} + \mathbf{v}_j; \mathbf{k}) &= U(\mathbf{r}; \mathbf{k}),\ j = 1, 2, \end{aligned} \tag{2.1}$$

where the operator $\mathcal{H}_{\mathbf{k}}$ is defined as

$$\mathcal{H}_{\mathbf{k}} = -\Delta - 2i\mathbf{k} \cdot \nabla + |\mathbf{k}|^2 + \delta V(\mathbf{r}). \tag{2.2}$$

The spectrum of the operator $\mathcal{H}_{\mathbf{k}}$ is discrete, i.e.,

$$\sigma(\mathcal{H}_{\mathbf{k}}) = \bigcup_{n \geq 1} \mu^{(n)}(\mathbf{k});$$

they can be ordered as

$$\mu^{(1)}(\mathbf{k}) \le \mu^{(2)}(\mathbf{k}) \le \mu^{(3)}(\mathbf{k}) \le \cdots .$$

$\mu^{(n)}(\mathbf{k})$ as a function of $\mathbf{k}$ is called the nth band of the dispersion relation. $\mu^{(n)}(\mathbf{k})$ is continuous and periodic, i.e., $\mu^{(n)}(\mathbf{k}+\mathbf{k}_l) = \mu^{(n)}(\mathbf{k})$, $l = 1, 2$. As $\mathbf{k}$ varies over the Brillouin zone Ω', the range of each branch $\mu^{(n)}(\mathbf{k})$ is a closed interval of the real axis. The spectrum of the Schrödinger operator $\mathcal{H}$ is the union of these intervals,

$$\sigma(\mathcal{H}) = \bigcup_{n\ge 1} \left\{ \mu^{(n)}(\mathbf{k}) : \mathbf{k} \in \Omega' \right\}. \tag{2.3}$$

Thus, the spectrum has a *band structure*. The adjunct intervals can sometimes overlap each other, which results in *band intersection*. In some cases, there can exist a gap between two adjunct intervals, which is termed a *band gap*. The corresponding Bloch modes are also indexed by n, and the Bloch modes $\{\varphi^{(n)}(\mathbf{k}) = e^{i\mathbf{k}\cdot\mathbf{r}} U^{(n)}(\mathbf{r};\mathbf{k}) : n \ge 1;\ \mathbf{k} \in \Omega'\}$ are complete in $L^2(\mathbb{R}^2)$. It is noted that each band $\mu^{(n)}(\mathbf{k})$ is continuous in $\mathbf{k}$ but is usually not analytic, e.g., at the intersection points. An explicit construction of the dispersion relation and corresponding Bloch modes is not known in the general case. However, in the tight-binding limit $\delta \gg 1$ and shallow potential limit $\delta \ll 1$, explicit results can be found via perturbation theory.

Regarding the HC lattices, the dispersion bands $\mu^{(1)}(\mathbf{k})$ and $\mu^{(2)}(\mathbf{k})$ behave in a conical manner near the Dirac points: $\mathbf{K} = \frac{1}{3}(\mathbf{k}_1 - \mathbf{k}_2)$, $\mathbf{K}' = \frac{1}{3}(\mathbf{k}_2 - \mathbf{k}_1)$. In the tight-binding limit δ, it has been shown that the dispersion relation has the expansion $\mu_{1,2}(\mathbf{k}) \sim \mu_0 \pm \frac{\sqrt{3}\tau l}{2}|\mathbf{k} - \mathbf{K}|$ to leading order where τ is a constant, which is called nearest neighbor hopping energy [30]. This conical behavior is not found in simple two-dimensional lattices. In the next section we examine the dispersion relation at the Dirac points in the shallow lattice limit: $\delta \ll 1$.

3. Bloch modes at Dirac points in shallow HC lattices. If the potential intensity is very large, i.e., $\delta \gg 1$, called the tight-binding limit, the Bloch modes are localized at the minima, and they can be well approximated by the superposition of orbitals. In this paper, we consider the opposite limit $\delta \ll 1$, sometimes called the nearly free limit; here all Bloch modes are represented by plane waves (see below). The linear perturbation theory for generic two-dimensional shallow periodic potentials is standard (see, for example, [33]). In this section we will analyze perturbation theory for the HC lattice at special points, which is important for our subsequent study of nonlinear wave dynamics. At these points there is degeneracy; the linear perturbation theory is nontrivial and must be done carefully.

Define another operator,

$$\mathcal{L}_{\mathbf{k}} = -\Delta - 2i\mathbf{k}\cdot\nabla + |\mathbf{k}|^2.$$

Since $\delta \ll 1$, the Schrödinger operator $\mathcal{H}_{\mathbf{k}}$ can be treated as a perturbation of the operator $\mathcal{L}_{\mathbf{k}}$. Note that all eigenfunctions are in the function space $L^2_{per}(\Omega)$ and the derivatives are in the weak sense.

For convenience, we will take $k_0 = 1$. If $k_0 \ne 1$, one can define new scales $\tilde{\mathbf{r}} = k_0\mathbf{r}$, $\tilde{\sigma} = \frac{\sigma}{k_0^2}$, and $\tilde{z} = zk_0^2$ so that the equation in the new coordinates is invariant. When $k_0 = 1$, the lattice scale is $|\mathbf{v}_1| = |\mathbf{v}_2| = \frac{4\pi}{3}$. Appropriate initial conditions should take this moderate number into account when doing computational simulations.

We then expand the eigenvalue μ and eigenfunction U in an expansion in δ,

$$\mu = \mu_0 + \delta\mu_1 + \delta^2\mu_2 + \cdots, \qquad U = U_0 + \delta U_1 + \delta^2 U_2 + \cdots,$$

where $U_s \in L^2_{per}(\Omega)$, $s = 0, 1, 2, 3, \ldots$. To simplify notation we have omitted the superscript since we are interested in the lowest eigenvalue, or eigenvalues if degeneracy is involved.

Substituting the Taylor expansions of μ and U into the eigenvalue problem (2.1) yields the following hierarchy of the equations:

$$\mathcal{O}(1) : (\mathcal{L}_{\mathbf{k}} - \mu_0)U_0 = 0, \tag{3.1}$$

$$\mathcal{O}(\delta) : (\mathcal{L}_{\mathbf{k}} - \mu_0)U_1 = -V(\mathbf{r})U_0 + \mu_1 U_0 := F_1, \tag{3.2}$$

$$\mathcal{O}(\delta^2) : (\mathcal{L}_{\mathbf{k}} - \mu_0)U_2 = -V(\mathbf{r})U_1 + \mu_2 U_0 + \mu_1 U_1 := F_2, \tag{3.3}$$

$$\mathcal{O}(\delta^n) : (\mathcal{L}_{\mathbf{k}} - \mu_0)U_n = -V(\mathbf{r})U_{n-1} + \sum_{m=0}^{n} \mu_m U_{n-m} := F_n. \tag{3.4}$$

For our purposes it is sufficient to expand the hierarchy to the order $\mathcal{O}(\delta^2)$.

As mentioned above we do not investigate general values of $\mathbf{k}$ in the Brillouin zone. Rather we study two special points, called Dirac points, $\mathbf{K} = \frac{1}{3}(\mathbf{k}_1 - \mathbf{k}_2)$ and $\mathbf{K}' = \frac{1}{3}(\mathbf{k}_2 - \mathbf{k}_1)$. They lie at the corners of Wigner–Seitz cell (see Figure 2.1(b)). Due to the underlying symmetries in HC lattices, the dispersion relation at these two points has degeneracies which will be shown below. We obtain the result associated with $\mathbf{k} = \mathbf{K}$; the result associated with $\mathbf{k} = \mathbf{K}'$ is similar.

3.1. Solutions to the order $\mathcal{O}(1)$ equation. Recall that we are studying the case where $\mathbf{k} = \mathbf{K}$ and $k_0 = 1$. Substituting the form

$$U_0 = e^{i(m\mathbf{k}_1 + n\mathbf{k}_2)\cdot\mathbf{r}},$$

where $m, n \in \mathbb{Z}$, into (3.1) yields after some manipulation

$$(3m - 3n + 2)^2 + 3(m + n)^2 = 4\mu_0.$$

There are infinitely many values of μ_0 for different choices of (m, n). Each value is a leading order value of a dispersion band. Since here we are interested in the lowest band dynamics, we take only the smallest value for μ_0. It can be seen that the minimum value of μ_0 is $\mu_0 = 1$, which is obtained when $(m, n) = (0, 0)$, $(-1, 0)$, $(0, 1)$, and the next one is $\mu_0 = 4$.

To clarify the situation, the eigenvalues are written as

$$\mu_0^{(1)} = \mu_0^{(2)} = \mu_0^{(3)} < \mu_0^{(4)} \leq \cdots,$$

where we note that the eigenvalues $\mu^{(1)}, \mu^{(2)}, \mu^{(3)}$ are the same at order $\mathcal{O}(1)$. The corresponding eigenfunctions are of the form

$$U_0 = C_0 + C_1 e^{-i\mathbf{k}_1\cdot\mathbf{r}} + C_2 e^{i\mathbf{k}_2\cdot\mathbf{r}},$$

where C_0, C_1, C_2 are arbitrary constants and will be determined at subsequent orders. The eigenvalue μ_0 has threefold degeneracy. Namely, the eigenspace of $\mathcal{L}_{\mathbf{K}}$ corresponding to $\mu_0 = 1$, i.e., the kernel of $\mathcal{L}_{\mathbf{K}} - \mu_0$, is a three-dimensional subspace of $L^2_{per}(\Omega)$. We denote it as

$$\mathbb{E} = \text{Span}\left\{1, e^{-i\mathbf{k}_1\cdot\mathbf{r}}, e^{i\mathbf{k}_2\cdot\mathbf{r}}\right\}.$$

Since the leading order eigenvalues of $\mathcal{H}_{\mathbf{K}}$ are equal, we continue to higher order to distinguish them. We consider the lowest three eigenvalues together due to the degeneracy.

3.2. Solutions to order $\mathcal{O}(\delta)$ equation. The leading order eigenvalue has multiplicity 3, in other words, the difference among $\mu^{(1)}, \mu^{(2)}, \mu^{(3)}$ is order $\mathcal{O}(\delta)$, so we continue to higher orders to see whether/how the eigenvalue splits upon perturbation.

The forcing term on the right-hand side of $\mathcal{O}(\delta)$, equation (3.2), is

$$F_1 = (-V(\mathbf{r}) + \mu_1)(C_0 + C_1 e^{-i\mathbf{k}_1\cdot\mathbf{r}} + C_2 e^{i\mathbf{k}_2\cdot\mathbf{r}}).$$

The Fredholm alternative requires the following three solvability conditions:

$$\langle F_1, 1\rangle = 0, \quad \langle F_1, e^{-i\mathbf{k}_1\cdot\mathbf{r}}\rangle = 0, \quad \langle F_1, e^{i\mathbf{k}_2\cdot\mathbf{r}}\rangle = 0, \tag{3.5}$$

where we define the inner product in $L^2_{per}(\Omega)$,

$$\langle f, g\rangle = \frac{1}{|\Omega|}\int_\Omega f(\mathbf{r})\overline{g(\mathbf{r})}d\mathbf{r},$$

and $\overline{g(\mathbf{r})}$, hereinafter, means the complex conjugate of $g(\mathbf{r})$ and $|\Omega|$ is the area of the unit cell Ω.

After some calculation the three solvability conditions lead to the following linear matrix problem:

$$\begin{pmatrix} \mu_1 & -1 & -1 \\ -1 & \mu_1 & -1 \\ -1 & -1 & \mu_1 \end{pmatrix} \begin{pmatrix} C_0 \\ C_1 \\ C_2 \end{pmatrix} = \begin{pmatrix} 0 \\ 0 \\ 0 \end{pmatrix}. \tag{3.6}$$

The above matrix problem has nontrivial solutions if and only if the determinant of the matrix is zero. Then we get

$$\mu_1^3 - 3\mu_1 - 2 = 0. \tag{3.7}$$

It has a simple root 2 and a double root -1. We denote $\mu_1^{(1)} = \mu_1^{(2)} = -1$ and $\mu_1^{(3)} = 2$.

The three-dimensional eigenspace $\mathbb{E}$ is decomposed into the direct sum of two subspaces under perturbation. Namely, there is a one-dimensional eigenspace which corresponds to $\mu_1^{(3)} = 2$ and a two-dimensional eigenspace which corresponds to $\mu_1^{(1)} = \mu_1^{(2)} = -1$.

Solving the above matrix problem (3.6) yields the corresponding eigenfunctions. For $\mu_1^{(1)} = \mu_1^{(2)} = -1$, we obtain two linearly independent eigenfunctions,

$$U_0^{(1)} = \frac{\sqrt{3}}{3}(1 + \eta e^{-i\mathbf{k}_1\cdot\mathbf{r}} + \bar{\eta} e^{i\mathbf{k}_2\cdot\mathbf{r}}), \tag{3.8}$$

$$U_0^{(2)} = \frac{\sqrt{3}}{3}(1 + \bar{\eta} e^{-i\mathbf{k}_1\cdot\mathbf{r}} + \eta e^{i\mathbf{k}_2\cdot\mathbf{r}}), \tag{3.9}$$

where $\eta = e^{\frac{2\pi i}{3}}$ and $\bar{\eta} = e^{-\frac{2\pi i}{3}}$.

For $\mu_1^{(3)} = 2$, we find the eigenfunction, which is

$$U_0^{(3)} = \frac{\sqrt{3}}{3}(1 + e^{-i\mathbf{k}_1\cdot\mathbf{r}} + e^{i\mathbf{k}_2\cdot\mathbf{r}}). \tag{3.10}$$

It can be verified that the above eigenfunctions are orthonormal, i.e.,

$$\langle U_0^{(m)}, U_0^{(n)}\rangle = \delta_{mn}, \quad m, n = 1, 2, 3.$$

In addition, the following orthonormal relations hold:

$$\langle V(\mathbf{r})U_0^{(m)}, U_0^{(n)}\rangle = \mu_1^{(m)}\delta_{mn}, \quad m,n=1,2,3, \tag{3.11}$$

which is directly from the solvability conditions (3.5). We will see that the above eigenfunctions are convenient in the derivation of the envelope dynamics in the next section.

So far, we have obtained the lowest eigenvalues of $\mathcal{H}_{\mathbf{K}}$ to order $\mathcal{O}(\delta)$. At leading order, the eigenvalues are the same, so the eigenspaces are mixed together and form a three-dimensional nullspace of $\mathcal{L}_{\mathbf{K}} - \mu_0$. But at order $\mathcal{O}(\delta)$ this nullspace splits into a direct sum of a one-dimensional eigensubspace and a two-dimensional eigensubspace; namely,

$$\mathbb{E} = \mathbb{E}_1 \oplus \mathbb{E}_2 = \text{Span}\left\{U_0^{(1)}, U_0^{(2)}\right\} \oplus \text{Span}\left\{U_0^{(3)}\right\}.$$

So, at order $\mathcal{O}(\delta)$ we can now distinguish between the eigenvalues which were equal at $\mathcal{O}(\delta)$. However, the eigenspaces for the first two eigenvalues are still mixed.

In order to get $U_1(\mathbf{r})$, we need to solve the inhomogeneous equation (3.2). Due to the Fredholm alternative there exists a unique solution in $\mathbb{E}^\perp$ (the orthogonal complement of $\mathbb{E}$ in $L^2(\mathbb{R}^2)$) for a given $U_0(\mathbf{r}) \in \mathbb{E}_1$ or $U_0(\mathbf{r}) \in \mathbb{E}_2$. Without loss of generality, we restrict $U_1 \in \mathbb{E}^\perp$ and take the homogeneous solution to vanish. Then we can define the inverse operator $(\mathcal{L}_K - \mu_0)^{-1} : \mathbb{E}^\perp \to \mathbb{E}^\perp$. And for any $f(\mathbf{r}) = \sum'_{m,n} \hat{f}_{m,n} e^{i(m\mathbf{k}_1 + n\mathbf{k}_2)\cdot\mathbf{r}} \in \mathbb{E}^\perp$

$$(\mathcal{L}_{\mathbf{K}} - \mu_0)^{-1} f = \sum_{m,n}{}' \frac{4\hat{f}_{m,n}}{(3m-3n+2)^2 + 3(m+n)^2 - 4\mu_0} e^{i(m\mathbf{k}_1 + n\mathbf{k}_2)\cdot\mathbf{r}},$$

where $\sum'_{m,n}$ means the sum excludes $(m,n) = (0,0), (-1,0), (1,0)$.

We denote

$$U_1^{(s)} = (\mathcal{L}_{\mathbf{K}} - \mu_0)^{-1}\left[\left(\mu_1^{(s)} + V(\mathbf{r})\right)U_0^{(s)}\right], \quad s = 1,2,3.$$

Since we have encountered eigenspace splitting, we need to consider the two cases separately.

The lowest three eigenvalues of problem (2.1), counting the multiplicity, have the forms $\mu^{(1)} = 1 - \delta + \mathcal{O}(\delta^2)$, $\mu^{(2)} = 1 - \delta + \mathcal{O}(\delta^2)$, and $\mu^{(3)} = 1 + 2\delta + \mathcal{O}(\delta^2)$. Thus $\mu^{(3)}$ separates from $\mu^{(1)}$ and $\mu^{(2)}$ at order $\mathcal{O}(\delta)$, while $\mu^{(1)}$ and $\mu^{(2)}$ remain equal.

Since the first two eigenvalues $\mu^{(1)}$ and $\mu^{(2)}$ are the same at this order, their corresponding eigenspaces do not separate. The associated eigenfunction has, at order $\mathcal{O}(1)$, the forms

$$U_0 = \alpha_1 U_0^{(1)} + \alpha_2 U_0^{(2)}, \tag{3.12}$$

and at order $\mathcal{O}(\delta)$

$$U_1 = \alpha_1 U_1^{(1)} + \alpha_2 U_1^{(2)}, \tag{3.13}$$

where α_1, α_2 are constants.

The eigenfunction for $\mu^{(3)}$ at the first two orders are

$$U_0 = \alpha_3 U_0^{(3)},$$
$$U_1 = \alpha_3 U_1^{(3)}.$$

3.3. Solutions to order $\mathcal{O}(\delta^2)$ equation. In this section, we investigate whether the eigenvalues $\mu^{(1)}$ and $\mu^{(2)}$, which are equal at order $\mathcal{O}(\delta)$, separate at $\mathcal{O}(\delta^2)$.

Substituting (3.12) and (3.13) into (3.3) and using the solvability conditions yields

$$\begin{pmatrix} \mu_2 + \frac{2}{3} & 0 \\ 0 & \mu_2 + \frac{2}{3} \end{pmatrix} \begin{pmatrix} \alpha_1 \\ \alpha_2 \end{pmatrix} = \begin{pmatrix} 0 \\ 0 \end{pmatrix}. \tag{3.14}$$

Note that there are three solvability conditions. However, the orthogonality to $U_0^{(3)}$ turns out to be a compatibility condition which is satisfied automatically. In addition, we have used the following relation:

$$\langle (\mu_1^{(m)} - V(\mathbf{r}))U_1^{(m)}, U_0^{(n)} \rangle = \frac{2}{3}\delta_{mn}, \quad m, n = 1, 2, 3, \tag{3.15}$$

which can be verified for the HC lattice (1.2).

The existence of the nontrivial solutions yields a double root $\mu_2^{(1)} = \mu_2^{(2)} = -2/3$. So the two-dimensional eigenspace at order $\mathcal{O}(\delta^2)$ does not split. In other words, the lowest eigenvalue of $\mathcal{H}_{\mathbf{k}}$ is degenerate to order $\mathcal{O}(\delta^2)$ at $\mathbf{k} = \mathbf{K}$.

Similarly, for $\mu_1^{(3)} = -2$, we only use the orthogonality to $U_0^{(3)}$ and get $\mu_2^{(3)} = -5/3$. Note that the orthogonality to $U_0^{(1)}$ and $U_0^{(2)}$ is automatically satisfied.

From the Fredholm condition, we can define the functions

$$U_2^{(s)} = (\mathcal{L}_K - \mu_0)^{-1} \left[(\mu_1^{(s)} - V(\mathbf{r}))U_1^{(1)} + \mu_2^{(s)} U_0^{(1)} \right], \quad s = 1, 2, 3.$$

Then the corresponding eigenfunction of $\mu_2^{(1)} = \mu_2^{(2)} = -2/3$ at order $\mathcal{O}(\delta^2)$ has the form

$$U_2 = \alpha_1 U_2^{(1)} + \alpha_2 U_2^{(2)},$$

and the corresponding eigenfunction $\mu_2^{(3)} = -5/3$ has the form

$$U_2 = \alpha_3 U_2^{(3)}.$$

3.4. Bloch mode structure. So far we have explicitly solved the eigenvalue problem of the operator $\mathcal{H}_{\mathbf{k}}$ to order $\mathcal{O}(\delta^2)$ at $\mathbf{k} = \mathbf{K}$. To order $\mathcal{O}(\delta^2)$, the operator $\mathcal{H}_{\mathbf{K}}$ has three discrete eigenvalues, $\mu^{(1)} = 1 - \delta - \frac{2}{3}\delta^2 + \mathcal{O}(\delta^3)$, $\mu^{(2)} = 1 - \delta - \frac{2}{3}\delta^2 + \mathcal{O}(\delta^3)$, and $\mu^{(3)} = 1 + 2\delta - \frac{5}{3}\delta^2 + \mathcal{O}(\delta^3)$. As discussed above, the lowest two eigenvalues, $\mu^{(1)}$ and $\mu^{(2)}$, are the same at this order. The eigenspaces corresponding to the two eigenvalues are mixed. In other words, the lowest eigenvalue is degenerate to order $\mathcal{O}(\delta^2)$, and the eigenspace corresponding to the eigenvalue $\mu = 1 - \delta - \frac{2}{3}\delta^2 + \mathcal{O}(\delta^3)$ is two-dimensional. The corresponding Bloch modes to order $\mathcal{O}(\delta^2)$ are

$$\varphi^{(1)}(\mathbf{r}) = e^{i\mathbf{K}\cdot\mathbf{r}} \left(U_0^{(1)} + \delta U_1^{(1)} + \delta^2 U_2^{(1)} \right) + \mathcal{O}(\delta^3),$$
$$\varphi^{(2)}(\mathbf{r}) = e^{i\mathbf{K}\cdot\mathbf{r}} \left(U_0^{(2)} + \delta U_1^{(2)} + \delta^2 U_2^{(2)} \right) + \mathcal{O}(\delta^3).$$

The eigenspace corresponding to the next higher eigenvalue, $\mu = 1 + 2\delta - \frac{5}{3}\delta^2 + \mathcal{O}(\delta^3)$, is one-dimensional and the corresponding Bloch mode is

$$\varphi^{(3)}(\mathbf{r}) = e^{i\mathbf{K}\cdot\mathbf{r}} \left(U_0^{(3)} + \delta U_1^{(3)} + \delta^2 U_2^{(3)} \right) + \mathcal{O}(\delta^3).$$

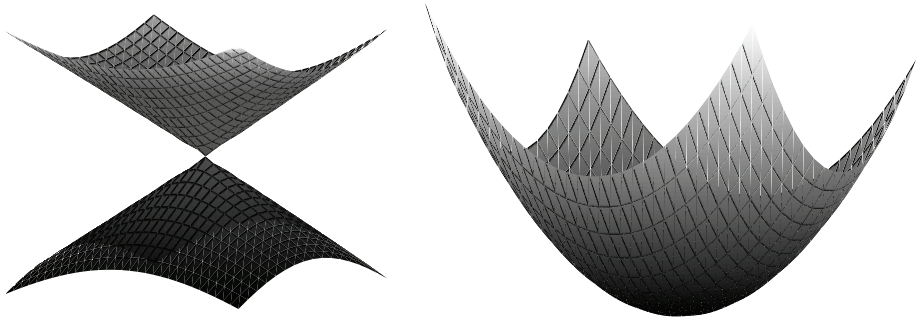

FIG. 3.1. *The dispersion surfaces* (a) $\mu^{(1)}(\mathbf{k}), \mu^{(2)}(\mathbf{k})$ *and* (b) $\mu^{(3)}(\mathbf{k})$ *in the vicinity of* $\mathbf{K}$ *when* $\delta = 0.4$. $\mu^{(1)}(\mathbf{k})$ *and* $\mu^{(2)}(\mathbf{k})$ *touch each other at the Dirac point* $\mathbf{K}$.

In principle, we can solve the perturbation hierarchy to any order in δ. However, this is out of the scope of this paper. From the quantities

$$\mu_n^{(s)} = \langle V(\mathbf{r}) U_{n-1}^{(s)}, U_0^{(s)} \rangle,$$
$$U_n^{(s)} = (\mathcal{L}_K - \mu_0)^{-1} \left[(\mu_1^{(s)} - V) U_{n-1}^{(s)} + \sum_{m=2}^{n} \mu_m U_{n-m} \right]$$

we conjecture that $\mu_n^{(1)} = \mu_n^{(2)}$ for all $n \geq 1$ and indeed for any finite value of δ. This conjecture is supported by careful numerical simulations. Our simulations show that $|\mu^{(2)} - \mu^{(1)}|$ has the same order as our numerical accuracy, which is $\mathcal{O}(10^{-11})$ for any δ. The conjecture means that the lowest eigenvalue of the operator $\mathcal{H}_{\mathbf{K}}$ with an HC lattice is degenerate with a multiplicity 2. To the best of our knowledge, this conjecture has not yet been rigorously proven. In this paper, we do not need the full description of the eigenvalue problem at any order. The description up to the order $\mathcal{O}(\delta^2)$ is sufficient for our requirements.

Since here we wish to study the dynamics in the vicinity of Dirac points, the Bloch mode structure at a general point in the Brillouin zone Ω' is not considered. The Bloch mode structure at the other Dirac point $\mathbf{k} = \mathbf{K}'$ can be obtained similarly and is omitted in this paper. We also note that the Taylor expansion of the linear dispersion relation $\mu(\mathbf{k})$ around a point $\mathbf{k}_0$ is closely related to the linear part of the corresponding envelope equations. So we included the calculation of $\mu(\mathbf{k})$ when $|\mathbf{k} - \mathbf{K}| \ll 1$ in section 5.

The dispersion surfaces $\mu^{(1)}(\mathbf{k}), \mu^{(2)}(\mathbf{k}), \mu^{(3)}(\mathbf{k})$ in the neighborhood of $\mathbf{K}$ are calculated numerically. The numerical scheme used here is the Fourier–Galerkin method. It converts the differential operator eigenvalue problem to a finite matrix eigenvalue problem by truncating the number of Fourier modes of eigenfunctions to a finite number; see, for example, [11, 12]. The results are shown in Figure 3.1. We see that the first two bands intersect with each other at the Dirac point $\mathbf{K}$. The third dispersion surface, which is distinct, lies above the first two. The analytical structure of the dispersion surfaces are explained further in section 5.

We can also support our analysis with a numerical comparison. In Figure 3.2, we plot the residual between the "true" eigenvalue obtained from a numerical simulation and the analytical result up to order $\mathcal{O}(\delta^2)$. Since our analysis is accurate to order

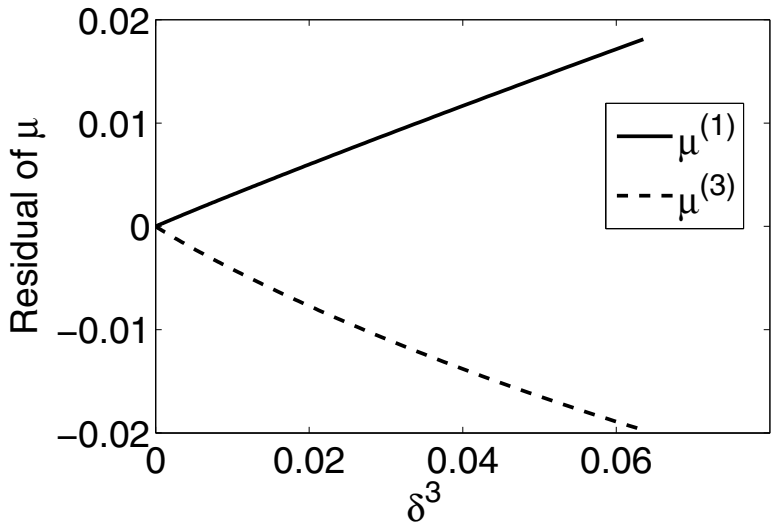

FIG. 3.2. *The residual of the dispersion relation, i.e., the difference between direct numerical simulation and the asymptotic results at the Dirac point. The solid line corresponds to* $\mu^{(1)}$ $(= \mu^{(2)})$ *and the dashed line corresponds to* $\mu^{(3)}$. *This relation suggests our asymptotic result is accurate to order* $\mathcal{O}(\delta^2)$.

$\mathcal{O}(\delta^2)$, the residuals should be order $\mathcal{O}(\delta^3)$. We can see that the dependence of residuals on δ^3 is, in fact, roughly linear.

4. Envelope wave dynamics at the Dirac points. In many applications, researchers are interested in the macroscopic dynamics of one or several Bloch envelopes. The original equation (1.1) governs the dynamics of all Bloch components and contains both lattice and envelope scales. So homogenized equations are often derived to describe and provide insight into the macroscopic dynamics. In HC lattices, we will focus on the dynamics of the envelopes associated with the Dirac points. With the analytic knowledge of the Bloch modes at the Dirac points, developed in the previous section, the envelope equations can be derived by the method of multiple scales.

We employ the transformation

$$\psi = \tilde{\psi} e^{i\mathbf{K}\cdot\mathbf{r} - i\mu_0 z} \tag{4.1}$$

and assume $\tilde{\psi}$ depends on slow scales as follows: $\tilde{\psi} = \tilde{\psi}(\mathbf{r}, \mathbf{R}, Z_1, Z_2)$, with $\mathbf{R} = \varepsilon\mathbf{r} = (X, Y)$, $Z_1 = \delta z$, $Z_2 = \delta^2 z$. It is noted that $\tilde{\psi}$ does not depend on the fast time z because we are only interested in the envelopes of the Bloch modes associated with the lowest eigenvalues $\mu^{(1)}$, $\mu^{(2)}$, $\mu^{(3)}$ and the components associated with higher eigenvalues are not included.

The equation for $\tilde{\psi}$ is

$$\left(\mathcal{L}_{\mathbf{K}} - \mu_0 + \delta V(\mathbf{r}) - i\delta\partial_{Z_1} - i\delta^2\partial_{Z_2} - 2\varepsilon(i\mathbf{K} + \nabla_{\mathbf{r}})\cdot\nabla_{\mathbf{R}} - \varepsilon^2\Delta_{\mathbf{R}}\right)\tilde{\psi} - \sigma|\tilde{\psi}|^2\tilde{\psi} = 0, \tag{4.2}$$

where $\nabla_{\mathbf{r}} = (\partial_x, \partial_y)$, $\nabla_{\mathbf{R}} = (\partial_X, \partial_Y)$, and $\Delta_{\mathbf{R}} = \partial_{XX} + \partial_{YY}$.

Then we expand the envelope $\tilde{\psi}$ in a series in δ:

$$\tilde{\psi} = \psi_0 + \delta\psi_1 + \delta^2\psi_2 + \cdots.$$

We will use the following integrals, which can be directly calculated:

$$\langle \nabla U_0^{(s)}, U_0^{(s)} \rangle = -i\mathbf{K}, \tag{4.3}$$

$$\langle \nabla U_0^{(1)}, U_0^{(2)} \rangle = \langle \nabla U_0^{(2)}, U_0^{(3)} \rangle = \langle \nabla U_0^{(3)}, U_0^{(1)} \rangle = \frac{1}{2}(-1, i), \tag{4.4}$$

$$\langle \nabla U_0^{(2)}, U_0^{(1)} \rangle = \langle \nabla U_0^{(1)}, U_0^{(3)} \rangle = \langle \nabla U_0^{(3)}, U_0^{(2)} \rangle = \frac{1}{2}(1, i). \tag{4.5}$$

Due to the cubic nonlinearity, we also need to compute the four wave mixing terms:

$$\frac{1}{|\Omega|}\int_\Omega U_0^{(s)} U_0^{(l)} \overline{U_0^{(p)} U_0^{(q)}} d\mathbf{r}, \quad s, l, p, q = 1, 2, 3.$$

Most of the integrals turn out to vanish except

$$\frac{1}{|\Omega|}\int_\Omega \left|U_0^{(s)}\right|^4 d\mathbf{r} = \frac{5}{3}, \quad s = 1, 2, 3,$$

$$\frac{1}{|\Omega|}\int_\Omega \left|U_0^{(s)}\right|^2 \left|U_0^{(l)}\right|^2 d\mathbf{r} = \frac{2}{3}, \quad s, l = 1, 2, 3,\ s \neq l,$$

$$\frac{1}{|\Omega|}\int_\Omega \left(U_0^{(s)}\right)^2 \overline{\left(U_0^{(l)} U_0^{(p)}\right)} d\mathbf{r} = \frac{1}{|\Omega|}\int_\Omega U_0^{(s)} U_0^{(l)} \overline{\left(U_0^{(p)}\right)^2} d\mathbf{r} = -\frac{1}{3}, \quad s \neq l \neq p.$$

Note that we are interested in the envelope dynamics associated with the lowest eigenvalues which at leading order has a threefold degeneracy. In this problem one has a number of different and interesting small parameter balances. Next we discuss two of them. We always balance the nonlinearity to the slow spatial parameter, i.e., $\varepsilon = |\sigma|$. We note that sometimes researchers take $\sigma = \pm 1$ and balance the slow spatial parameter with nonlinearity by scaling the amplitude of the envelope with an appropriate power of ε.

4.1. The case: $\boldsymbol{\varepsilon = |\sigma| = \delta}$. In this subsection we employ the balance of slow space, slow time, and nonlinearity.

Substituting the expansion for $\tilde{\psi}$ into (4.2) yields the following equations taken to $\mathcal{O}(\delta)$:

$$\begin{aligned}
&\mathcal{O}(1) : (\mathcal{L}_{\mathbf{K}} - \mu_0)\,\psi_0 = 0,\\
&\mathcal{O}(\delta) : (\mathcal{L}_{\mathbf{K}} - \mu_0)\,\psi_1 = -V(\mathbf{r})\psi_0 + i\partial_{Z_1}\psi_0 + 2(i\mathbf{K} + \nabla_{\mathbf{r}}) \cdot \nabla_{\mathbf{R}}\psi_0 + \operatorname{sgn}(\sigma)|\psi_0|^2\psi_0.
\end{aligned}$$

Solving the order $\mathcal{O}(1)$ equation yields

$$\psi_0 = A_1(\mathbf{R}, Z_1)U_0^{(1)} + A_2(\mathbf{R}, Z_1)U_0^{(2)} + A_3(\mathbf{R}, Z_1)U_0^{(3)}.$$

Here $A_s(\mathbf{R}, Z_1)$ are the envelopes associated with the three Bloch modes $\varphi^{(s)}$, $s = 1, 2, 3$. To solve the $\mathcal{O}(\delta)$ equation, we use the three solvability conditions, which yield the envelope equations

$$i\partial_{Z_1}A_1 + A_1 + \partial_+ A_2 + \partial_- A_3 + \operatorname{sgn}(\sigma)\Phi_1 = 0, \tag{4.6a}$$

$$i\partial_{Z_1}A_2 + A_2 + \partial_+ A_3 + \partial_- A_1 + \operatorname{sgn}(\sigma)\Phi_2 = 0, \tag{4.6b}$$

$$i\partial_{Z_1}A_3 - 2A_3 + \partial_+ A_1 + \partial_- A_2 + \operatorname{sgn}(\sigma)\Phi_3 = 0, \tag{4.6c}$$

where

$$\partial_- = (-\partial_X + i\partial_Y), \quad \partial_+ = (\partial_X + i\partial_Y),$$

and

$$\Phi_1 = \frac{1}{3}\left[\left(5|A_1|^2 + 4|A_2|^2 + 4|A_3|^2\right)A_1 - A_2^2\overline{A_3} - A_3^2\overline{A_2} - 2A_2A_3\overline{A_1}\right],$$
$$\Phi_2 = \frac{1}{3}\left[\left(5|A_2|^2 + 4|A_1|^2 + 4|A_3|^2\right)A_2 - A_1^2\overline{A_3} - A_3^2\overline{A_1} - 2A_1A_3\overline{A_2}\right],$$
$$\Phi_3 = \frac{1}{3}\left[\left(5|A_3|^2 + 4|A_1|^2 + 4|A_2|^2\right)A_3 - A_1^2\overline{A_2} - A_2^2\overline{A_1} - 2A_1A_2\overline{A_3}\right].$$

These equations are Dirac-type with suitable linear phase and nonlinear interaction terms; note that the A_3 component has a different phase correction term from the A_1 and A_2 components. We remark that even when there is no space variation the equations are not trivial due to the four wave interaction components. The differential equations for space-independent solutions are sometimes called *Landau equations*, which here describes certain nonlinear interband transitions.

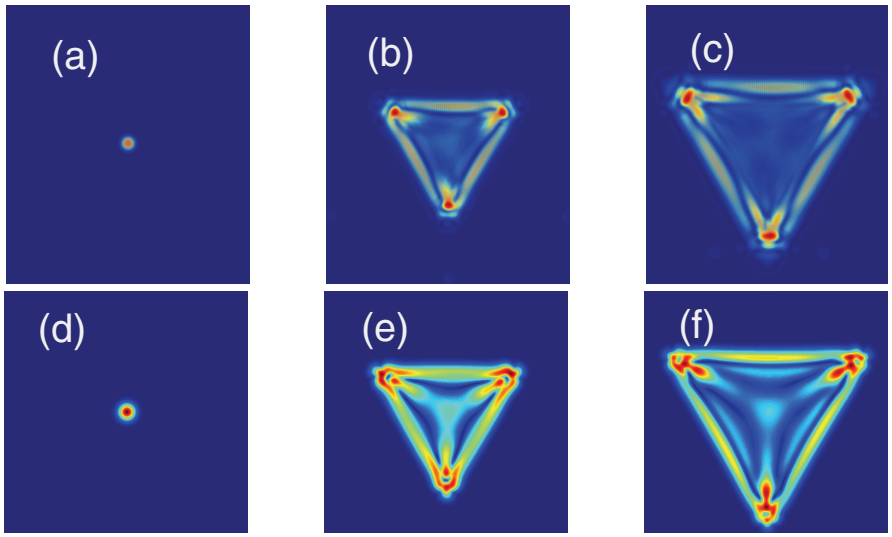

FIG. 4.1. *Numerical simulations of envelope dynamics in (top panels) the original NLS equation* (1.1) *and (bottom panels) the asymptotic Dirac system* (4.6).

To support our analysis, a numerical comparison is presented here. The numerical scheme used in this paper to integrate all evolution equations is the pseudospectral method in space with a fourth order Runge–Kutta method in time; see, for example, [12]. The initial condition we choose for the NLS equation (1.1) is always a wide gaussian multiplied by a Bloch mode. In the simulation of Figure 4.1, the initial condition for (1.1) is $\psi(\mathbf{r}, z = 0) = e^{-(X^2+Y^2)}U_0^{(1)}$. This initial condition corresponds to $A_1(\mathbf{R}, Z_1 = 0) = e^{-(X^2+Y^2)}$, $A_2(\mathbf{R}, Z_1 = 0) = A_3(\mathbf{R}, Z_1 = 0) = 0$. In Figure 4.1, the panels (a)–(c) show the intensity patterns of $\psi(\mathbf{r}, z)$ for different propagation distances with the above initial input. Here the parameters are $\delta = \varepsilon = \sigma = 0.2$. Panels (d)–(f) depict the intensity of the superposition of A_1, A_2, and A_3 at the corresponding propagation distances. From the figure, we see that an initial radially symmetric gaussian (for component A_1) separates into a triangular diffraction pattern.

In optics, this phenomenon is referred to as diffraction of propagating beams in a crystal with a transversely varying index of refraction. Figure 4.1 shows the pattern

of the diffraction when the incident beam is a superposition of three gaussian beams with input angles being $\mathbf{K}$, $\mathbf{K}-\mathbf{k}_1$, and $\mathbf{K}+\mathbf{k}_2$. Researchers can easily study the nonlinear diffraction patterns of other combinations of incident angles where the initial conditions of the envelope equation would be different.

4.2. The case: $\varepsilon = |\boldsymbol{\sigma}| = \boldsymbol{\delta^2}$. In this subsection we employ the balance of slow space and nonlinearity with δ^2. Substituting (4.1) into (1.1) yields the following hierarchy of equations to $\mathcal{O}(\delta^2)$:

$$\begin{aligned}
&\mathcal{O}(1) : (\mathcal{L}_{\mathbf{K}} - \mu_0)\,\psi_0 = 0,\\
&\mathcal{O}(\delta) : (\mathcal{L}_{\mathbf{K}} - \mu_0)\,\psi_1 = -V(\mathbf{r})\psi_0 + i\partial_{Z_1}\psi_0,\\
&\mathcal{O}(\delta^2) : (\mathcal{L}_{\mathbf{K}} - \mu_0)\,\psi_2 = -V(\mathbf{r})\psi_1 + i\partial_{Z_1}\psi_1 + i\partial_{Z_2}\psi_0 + 2(i\mathbf{K}+\nabla_{\mathbf{r}})\cdot\nabla_{\mathbf{R}}\psi_0 + \mathrm{sgn}(\sigma)|\psi_0|^2\psi_0.
\end{aligned}$$

Solving the hierarchy is similar to what was done above. The order $\mathcal{O}(1)$ equation gives us that

$$\psi_0 = \sum_{s=1}^{3} A_s(\mathbf{R}, Z_1, Z_2) U_0^{(s)}.$$

Fredholm conditions at $\mathcal{O}(\delta)$ give the Z_1 dependence of each envelope A_s. Namely,

$$i\partial_{Z_1} A_s - \mu_1^{(s)} A_s = 0, \quad s = 1, 2, 3,$$

where we have used the orthogonality relations (3.11). Thus we get

$$\psi_0 = \sum_{s=1}^{3} A_s(\mathbf{R}, Z_2) U_0^{(s)} e^{-i\mu_1^{(s)} Z_1}.$$

Solving the order $\mathcal{O}(\delta)$ equation we get

$$\psi_1 = \sum_{s=1}^{3} A_s(\mathbf{R}, Z_2) U_1^{(s)} e^{-i\mu_1^{(s)} Z_1}.$$

Note that the homogeneous solutions are chosen to be zero, and their effect can be included in higher order equations in the usual manner.

Using

$$\left\langle \left(\mu_1^{(m)} - V(\mathbf{r})\right) U_1^{(m)}, U_0^{(n)} \right\rangle = -\mu_2^{(m)} \delta_{mn}, \quad m, n = 1, 2, 3,$$

and applying the three solvability conditions at $\mathcal{O}(\delta^2)$ yields the following equations:

$$\begin{aligned}
&i\partial_{Z_2} A_1 + \frac{2}{3} A_1 + \partial_+ A_2 + \partial_- A_3 e^{-3iZ_2/\delta} + \mathrm{sgn}(\sigma)\tilde{\Phi}_1 = 0,\\
&i\partial_{Z_2} A_2 + \frac{2}{3} A_2 + \partial_+ A_3 e^{-3iZ_2/\delta} + \partial_- A_1 + \mathrm{sgn}(\sigma)\tilde{\Phi}_2 = 0,\\
&i\partial_{Z_2} A_3 - \frac{5}{3} A_3 + (\partial_+ A_1 + \partial_- A_2) e^{3iZ_2/\delta} + \mathrm{sgn}(\sigma)\tilde{\Phi}_3 = 0,
\end{aligned}$$

where

$$\begin{aligned}
\tilde{\Phi}_1 &= \frac{1}{3}\left[\left(5|A_1|^2 + 4|A_2|^2 + 4|A_3|^2\right) A_1 - A_2^2\overline{A_3} e^{3iZ_2/\delta} - A_3^2\overline{A_2} e^{-6iZ_2/\delta} - 2A_2A_3\overline{A_1} e^{-3iZ_2/\delta}\right],\\
\tilde{\Phi}_2 &= \frac{1}{3}\left[\left(5|A_2|^2 + 4|A_1|^2 + 4|A_3|^2\right) A_2 - A_1^2\overline{A_3} e^{3iZ_2/\delta} - A_3^2\overline{A_1} e^{-6iZ_2/\delta} - 2A_1A_3\overline{A_2} e^{-3iZ_2/\delta}\right],\\
\tilde{\Phi}_3 &= \frac{1}{3}\left[\left(5|A_3|^2 + 4|A_1|^2 + 4|A_2|^2\right) A_3 - A_1^2\overline{A_2} e^{3iZ_2/\delta} - A_2^2\overline{A_1} e^{3iZ_2/\delta} - 2A_1A_2\overline{A_3} e^{6iZ_2/\delta}\right].
\end{aligned}$$

In the above equations we see that there are rapidly varying terms. This is due to the dispersion relation being $\mu_1 = -1, -1, 2$ at $\mathcal{O}(\delta)$.

One can average out the fast phase (via another multiple scales procedure), and the equations reduce to

$$i\partial_{Z_2} A_1 + \frac{2}{3} A_1 + \partial_+ A_2 + \mathrm{sgn}(\sigma)\frac{1}{3}\left(5|A_1|^2 + 4|A_2|^2 + 4|A_3|^2\right) A_1 = 0, \tag{4.7}$$

$$i\partial_{Z_2} A_2 + \frac{2}{3} A_2 + \partial_- A_1 + \mathrm{sgn}(\sigma)\frac{1}{3}\left(5|A_2|^2 + 4|A_1|^2 + 4|A_3|^2\right) A_2 = 0, \tag{4.8}$$

$$i\partial_{Z_2} A_3 - \frac{5}{3} A_3 + \mathrm{sgn}(\sigma)\frac{1}{3}\left(5|A_3|^2 + 4|A_1|^2 + 4|A_2|^2\right) A_3 = 0. \tag{4.9}$$

Note that the A_3 equation is only a phase modulation. So if A_3 is initially zero, then it remains zero. In other words, if the A_3 component is initially much weaker than the A_1 and A_2 components, then we may consider the detached equations (4.7) and (4.8) alone without A_3.

Rescaling the phases of A_1 and A_2 (i.e., $\tilde{A}_s = A_s e^{-i\frac{2}{3}Z_2}$ and dropping the tilde above A_s) yields the following coupled nonlinear Dirac system:

$$i\partial_{Z_2} A_1 + \partial_+ A_2 + \mathrm{sgn}(\sigma)\frac{1}{3}\left(5|A_1|^2 + 4|A_2|^2\right) A_1 = 0, \tag{4.10a}$$

$$i\partial_{Z_2} A_2 + \partial_- A_1 + \mathrm{sgn}(\sigma)\frac{1}{3}\left(5|A_2|^2 + 4|A_1|^2\right) A_2 = 0. \tag{4.10b}$$

It is noted that the Dirac system can also be derived in the tight-binding limit. The equation in that limit is similar in that the linear terms are the same; however, the nonlinear terms are somewhat different [32].

This nonlinear Dirac system governs the dynamics of the envelopes associated with the lowest eigenvalues $\mu^{(1)}$ and $\mu^{(2)}$. We compare the dynamics between the original NLS equation (1.1) and the reduced Dirac equation (4.10) via numerical simulations. The initial condition for the original NLS equation (1.1) is still a gaussian: $\psi(\mathbf{r}, z = 0) = e^{-(X^2+Y^2)} U_0^{(1)}$ but now $\varepsilon = \delta^2 = \sigma = 0.2^2 = 0.04$. The numerical comparison shows very good agreement. For the envelope equations the initial conditions are that A_1 is a gaussian while A_2 is zero. Interestingly when A_1 is initially a unit gaussian and A_2 is a unit gaussian multiplied by a constant phase term, $e^{i\theta_0}$, a "notch" forms where the direction of the notch is determined by the phase θ_0; see Figure 4.2 below.

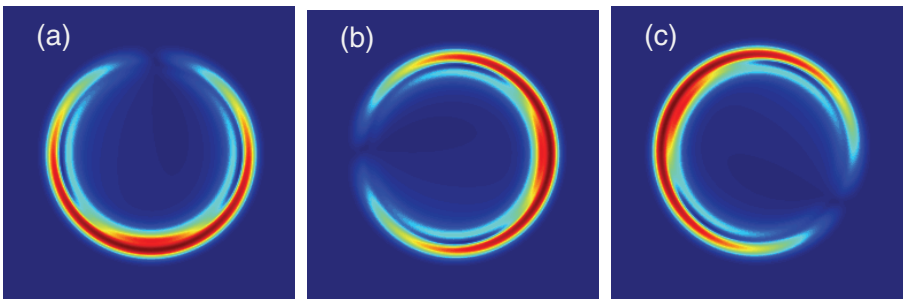

FIG. 4.2. *The conical diffraction with a "notch." Initially, A_1 is a unit gaussian, A_2 is a unit gaussian multiplied by $e^{i\theta_0}$, and θ_0 is a constant phase:* (a) 0; (b) $-\pi/2$; (c) $-2\pi/3$.

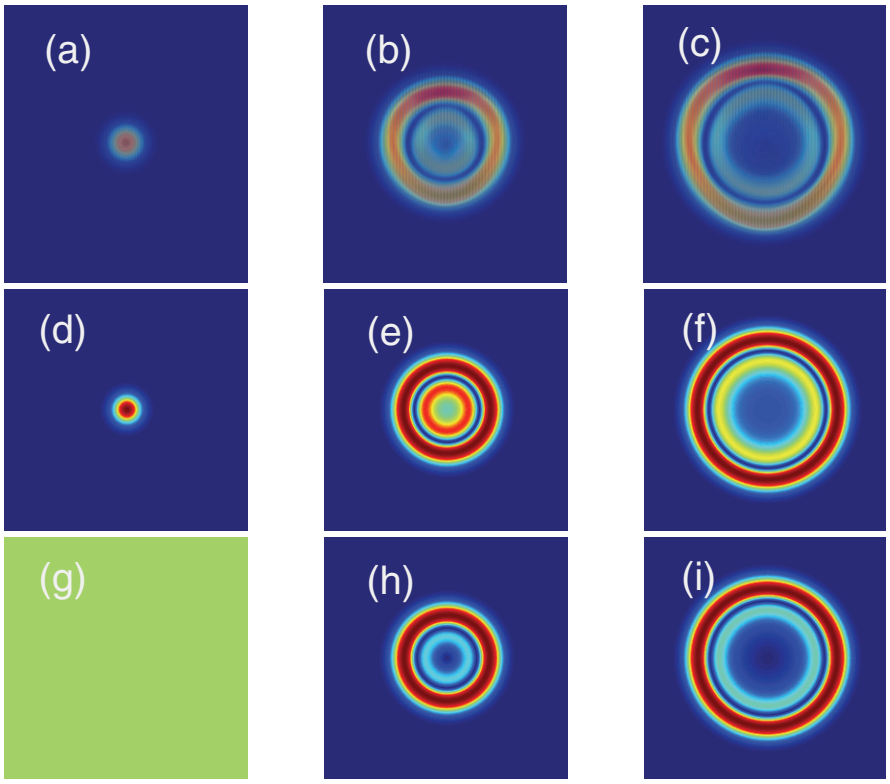

FIG. 4.3. *Numerical simulations of conical diffraction in (top panels) the original NLS equation* (1.1) *and (middle and bottom panels) the reduced Dirac system* (4.10). *Here* A_1 *is shown in the middle panels and* A_2 *is shown in the bottom panels.*

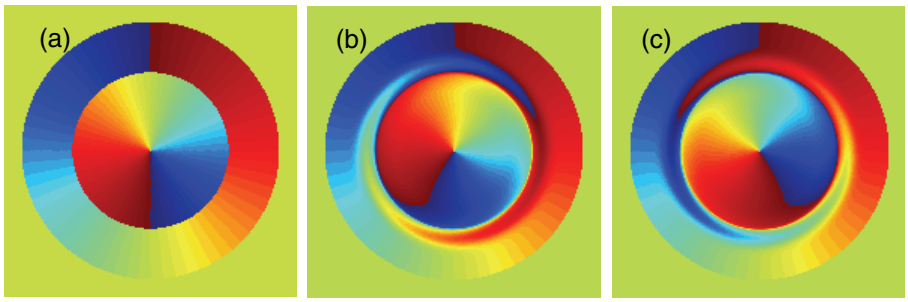

FIG. 4.4. *The phase comparison for linear and nonlinear Dirac equations.* (a) $sgn(\sigma) = 0$; (b) $sgn(\sigma) = 1$; (c) $sgn(\sigma) = -1$.

The above phenomenon shown in Figure 4.3 is called conical diffraction. Basically, conical diffraction is a linear phenomenon and corresponds to the dispersion relation being conical in the neighborhood of Dirac points. This weak nonlinearity has limited effects on the intensity of the envelope, but can affect the phase—see Figure 4.4. On the other hand, strong nonlinearity can change the diffraction pattern significantly [29, 35]. The detailed analysis is outside the scope of this paper.

5. Linear dispersion relations of the envelope equations. In the coupled mode system (4.6) at order $\mathcal{O}(\delta)$, neglecting the nonlinear terms and transforming to Fourier spectral space, i.e., $A_j \sim \hat{A}_j e^{-i\omega(\mathbf{q})Z_1 + i\mathbf{q}\cdot\mathbf{R}}$, yields

$$\begin{pmatrix} \omega+1 & \hat{\partial}_+ & \hat{\partial}_+ \\ \hat{\partial}_+ & \omega+1 & \hat{\partial}_- \\ \hat{\partial}_- & \hat{\partial}_- & \omega-2 \end{pmatrix} \begin{pmatrix} \hat{A}_1 \\ \hat{A}_2 \\ \hat{A}_3 \end{pmatrix} = \begin{pmatrix} 0 \\ 0 \\ 0 \end{pmatrix},$$

where $\hat{\partial}_+ = -iq_1 - q_2$ and $\hat{\partial}_- = iq_1 - q_2$. Here $\mathbf{q} = (q_1, q_2)$ is the Fourier wave vector of the envelope and $\omega(\mathbf{q})$ is the linear dispersion relation of the envelope equation.

The determinant of the above coefficient matrix gives the equation

$$(\omega+1)^2(\omega-2) - 2(\omega+1)(q_1^2+q_2^2) - (\omega-2)(q_1^2+q_2^2) - 2q_2(-3q_1^2+q_2^2) = 0. \tag{5.1}$$

Solving the above equation yields the envelope dispersion relation $\omega(\mathbf{q})$. Since the dispersion relation is represented by the roots of a cubic equation, it has three branches.

This envelope dispersion relation (the evolution of a Fourier mode) will give us the dispersion relation of the original eigenvalue problem (2.1), i.e., the evolution of a Bloch mode in the neighborhood of the Dirac point. The dispersion relations of the evolution system and the general dispersion relation are connected; we discuss this further. The original field of the lattice NLS equation has the form

$$\psi(r,z) = \sum_{s=1}^{3} A_s(\mathbf{R}, Z_1) U_0^{(s)} e^{i\mathbf{K}\cdot\mathbf{r} - i\mu_0 z} + \mathcal{O}(\delta).$$

The Bloch mode decomposition (similar to Fourier decomposition) gives the evolution of the field $\psi(r,z)$. Combining the Bloch mode decomposition of the original field and Fourier decomposition of the envelope yields that

$$\begin{aligned} &\varepsilon\mathbf{q} + \mathbf{K} = \mathbf{k}, \\ &\delta\omega(\mathbf{q}) + \mu_0 + \mathcal{O}(\delta^2) = \mu(\mathbf{k}). \end{aligned}$$

We have associated the Fourier wave vector of the envelopes, $\mathbf{q}$, with the Bloch wave vector $\mathbf{k}$ in the neighborhood of $\mathbf{K}$ as well as the dispersion relations.

Note that the envelope equation is based on the balance $\delta = \varepsilon$ with $\mathbf{q} = \frac{\mathbf{k}-\mathbf{K}}{\varepsilon}$. The dispersion relation obtained from (5.1) is valid for $|\mathbf{k}-\mathbf{K}| \sim \mathcal{O}(\delta)$.

If $\mathbf{q} = \mathbf{0}$, we get $\omega(\mathbf{0}) = -1, -1, 2$, which are exactly the order $\mathcal{O}(\delta)$ corrections to the lowest eigenvalues at $\mathbf{k} = \mathbf{K}$, i.e., $\mu_1^{(1)}, \mu_1^{(3)}, \mu_1^{(3)}$. If $|\mathbf{q}| = \sqrt{q_1^2+q_2^2} \sim \mathcal{O}(1)$, i.e., $|\mathbf{k}-\mathbf{K}| \sim \mathcal{O}(\delta)$, the branch that bifurcated from $\omega = 2$ can affect the branch that bifurcated from $\omega = -1$. In other words, the dispersion branch $\mu^{(3)}(\mathbf{k})$ can eventually intersect with the other dispersion relations branches $\mu^{(1)}(\mathbf{k}), \mu^{(2)}(\mathbf{k})$ of $\mathcal{H}_{\mathbf{K}}$ at some $\mathbf{k}$ which is not very close to $\mathbf{K}$. We also note that the intersection would occur away from the region depicted by Figure 3.1 with $\mu^{(3)}(\mathbf{k})$ lying above $\mu^{(1)}(\mathbf{k}), \mu^{(2)}(\mathbf{k})$.

If $|\mathbf{q}| \ll 1$, we can solve the above equation via perturbation theory. Since $\omega(\mathbf{0}) = 2$ is a simple root when $\mathbf{q} = \mathbf{0}$, the root to the above polynomial when $|\mathbf{q}| \ll 1$ is also simple and the dispersion relation is analytic [15]. Suppose the dispersion relation $\omega(\mathbf{q})$ has the expression $\omega(\mathbf{q}) = 2 + f$, where $f \ll 1$. Then we have

$$9f - 6(q_1^2+q_2^2) + \mathcal{O}((|\mathbf{q}|)^3) = 0,$$

and hence $f = \frac{2}{3}(q_1^2+q_2^2) + \mathcal{O}(|\mathbf{q}|^3)$.

Since the root $\omega(\mathbf{0}) = -1$ is a double root when $\mathbf{q} = \mathbf{0}$, the dispersion relation usually is no longer analytic [15]. We can see this here when $|\mathbf{q}| \ll 1$; we have $\omega(\mathbf{q}) = -1 + g$, where $g \ll 1$. Then we have

$$-3g^2 + 3(q_1^2 + q_2^2) + \mathcal{O}(|\mathbf{q}|^3) = 0,$$

and so $g^2 = q_1^2 + q_2^2 + \mathcal{O}(|\mathbf{q}|^3)$.

To summarize the above, we find that the dispersion relation $\mu^{(3)}(\mathbf{k})$ is analytic around $\mathbf{k} = \mathbf{K}$ and has the expansion

$$\mu^{(3)}(\mathbf{k}) = 1 + \delta\left(2 + \frac{2}{3}|\mathbf{k} - \mathbf{K}|^2 + \mathcal{O}(|\mathbf{k} - \mathbf{K}|^3)\right) + \mathcal{O}(\delta^2),$$

where $|\mathbf{k} - \mathbf{K}| \ll \delta$.

On the other hand the dispersion relations of $\mu^{(1)}(\mathbf{k})$ and $\mu^{(2)}(\mathbf{k})$ are not analytic around $\mathbf{k} = \mathbf{K}$; they have the expansions

$$\mu^{(1)}(\mathbf{k}) = 1 + \delta(-1 - |\mathbf{k} - \mathbf{K}| + \mathcal{O}(|\mathbf{k} - \mathbf{K}|^2)) + \mathcal{O}(\delta^2)$$

and

$$\mu^{(2)}(\mathbf{k}) = 1 + \delta(-1 + |\mathbf{k} - \mathbf{K}| + \mathcal{O}(|\mathbf{k} - \mathbf{K}|^2)) + \mathcal{O}(\delta^2),$$

where $|\mathbf{k} - \mathbf{K}| \ll \delta$.

The above analysis agrees with the direct numerical calculation of the dispersion surface which is shown in Figure 3.1. It is seen that $\mu^{(1)}(\mathbf{k})$ and $\mu^{(2)}(\mathbf{k})$ touch each other at the Dirac point $\mathbf{K}$, and the dispersion relation in the neighborhood of $\mathbf{K}$ is conical while $\mu^{(3)}(\mathbf{k})$ is analytic in the neighborhood of $\mathbf{K}$ and has a minimum at $\mathbf{k} = \mathbf{K}$. It is noted that envelope equations are consistent with the first two terms of Taylor expansion in $\mathbf{k} - \mathbf{K}$ of $\mu(\mathbf{k})$ around $\mathbf{K}$, and the expansion is accurate to order $\mathcal{O}(\delta^2)$. However, the nonlinear terms are not obtained from the Taylor expansion of the dispersion relation; they must be obtained separately, as we have done in section 4.

6. Conclusion. This paper investigates nonlinear waves in shallow (with scale δ) honeycomb lattices. The linear spectrum and corresponding Bloch structures at Dirac point $\mathbf{K}$ are studied. The dispersion relation has threefold degeneracy to leading order and splits to simple and double eigenvalues at the following order. It is shown that the degeneracy of the double eigenvalue holds at least to next order. Based on results in strong potential limit and numerical calculations, it is conjectured that the degeneracy persists for any order of perturbation—and indeed for any finite strength—δ of the potential.

The nonlinear wave envelope dynamics is found to depend on different asymptotic balances. In one case, when the scale of the envelope is order $\mathcal{O}(\delta)$, a three-level nonlinear Dirac-type equation is derived and triangular diffraction is found. When the scale of the envelope, ε is on the order $\mathcal{O}(\delta^2)$, a two-level nonlinear Dirac equation is derived, and conical diffraction is observed. The analysis agrees well with direct numerical simulations.

REFERENCES

[1] K. S. Novoselov, A. K. Geim, S. V. Morozov, D. Jiang, Y. Zhang, S. V. Dubonos, I. V. Grigorieva, and A. A. Firsov, *Electric field effect in atomically thin carbon films*, Science, 306 (2004), pp. 666–669.

[2] K. S. Novoselov, A. K. Geim, S. V. Morozov, D. Jiang, M. I. Katsnelson, I. V. Grigorieva, S. V. Dubonos, and A. A. Firsov, *Two-dimensional gas of massless Dirac fermions in graphene*, Nature, 438 (2005), pp. 197–200.
[3] S. L. Zhu, B. Wang, and L. M. Duan, *Simulation and detection of Dirac fermions with cold atoms in an optical lattice*, Phys. Rev. Lett., 98 (2007), 260402.
[4] L. H. Haddad and L. C. Carr, *The nonlinear Dirac equation in Bose-Einstein condensates: Foundation and symmetries*, Phys. D, 238 (2009), pp. 1413–1421.
[5] C. R. Rosberg, D. N. Neshev, A. A. Sukhorukov, W. Krolikowski, and Y. S. Kivshar, *Observation of nonlinear self-trapping in triangular photonic lattices*, Opt. Lett., 32 (2007), pp. 397–399.
[6] O. Peleg, G. Bartal, B. Freedman, O. Manela, M. Segev, and D. N. Christodoulides, *Conical diffraction and gap solitons in honeycomb photonic lattices*, Phys. Rev. Lett., 98 (2007), 103901.
[7] O. Bahat-Treidel, O. Peleg, and M. Segev, *Symmetry breaking in honeycomb photonic lattices*, Opt. Lett., 33 (2008), pp. 2251–2253.
[8] F. D. M. Haldane and S. Raghu, *Possible realization of directional optical waveguides in photonic crystals with broken time-reversal symmetry*, Phys. Rev. Lett., 100 (2008), 013904.
[9] C. Sulem and P. L. Sulem, *The Nonlinear Schrödinger Equation: Self-Focusing and Wave Collapse*, Springer, Berlin, 1999.
[10] T. Tao, *Nonlinear Dispersive Equations: Local and Global Analysis*, AMS, Providence, RI, 2006.
[11] M. Skorobogatiy and J. Yang, *Fundamentals of Photonic Crystal Guiding*, Cambridge University Press, New York, 2009.
[12] J. Yang, *Nonlinear Waves in Integrable and Nonintegrable Systems*, SIAM, Philadelphia, 2010.
[13] C. J. Pethick and H. Smith, *Bose-Einstein Condensation in Dilute Gases*, Cambridge University Press, New York, 2001.
[14] O. Morsch and M. Oberthaler, *Dynamics of Bose-Einstein condensates in optical lattices*, Rev. Modern Phys., 1 (2006), pp. 179–215.
[15] M. Reed and B. Simon, *Methods of Mathematical Physics* IV: *Analysis of Operators*, Academic Press, New York, 1978.
[16] F. Odeh and J. B. Keller, *Partial differential equations with periodic coefficients and Bloch waves in crystals*, J. Math. Phys., 5 (1964), pp. 1499–1503.
[17] C. Sparber, *Effective mass theorems for nonlinear Schrödinger equations*, SIAM J. Appl. Math., 66 (2006), pp. 820–842.
[18] M. J. Ablowitz and Y. Zhu, *Unified description of the dynamics of wave envelopes in two-dimensional simple periodic lattices*, Stud. Appl. Math. (submitted).
[19] R. H. Goodman, M. I. Weinstein, and P. J. Holmes, *Nonlinear propagation of light in one-dimensional periodic structures*, J. Nonlinear Sci., 11 (2001), pp. 123–168.
[20] G. Schneider and H. Uecker, *Nonlinear coupled mode dynamics in hyperbolic and parabolic periodically structured spatially extended systems*, Asymptot. Anal., 28 (2001), pp. 163–180.
[21] A. B. Aceves, B. Costantini, and C. De Angelis, *Two-dimensional gap solitons in a nonlinear periodic slab waveguide*, J. Opt. Soc. Amer. B Opt. Phys., 12 (1995), pp. 1475–1479.
[22] T. Dohnal and A. B. Aceves, *Optical soliton bullets in* $(2+1)D$ *nonlinear Bragg resonant periodic geometries*, Stud. Appl. Math., 115 (2005), pp. 209–232.
[23] D. Agueev and D. Pelinovsky, *Modeling of wave resonances in low-contrast photonic crystals*, SIAM J. Appl. Math., 65 (2005), pp. 1101–1129.
[24] Z. Shi and J. Yang, *Solitary waves bifurcated from Bloch-band edges in two-dimensional periodic media*, Phys. Rev. E, 75 (2007), 056602.
[25] T. Dohnal, D. Pelinovsky, and G. Schneider, *Coupled-mode equations and gap solitons in a two-dimensional nonlinear elliptic problem with a separable periodic potential*, J. Nonlinear Sci., 19 (2009), pp. 95–131.
[26] D. Dohnal and H. Uecker, *Coupled-mode equations and gap solitons for the* $2d$ *Gross-Pitaevskii equation with a non-separable periodic potential*, Phys. D, 238 (2009), pp. 860–879.
[27] B. Ilan and M. I. Weinstein, *Band-edge solitons, nonlinear Schrödinger/Gross–Pitaevskii equations, and effective media*, Multiscale Model. Simul., 8 (2010), pp. 1055–1101.
[28] V. S. Shchesnovich, A. S. Desyatnikov, and Y. S. Kivshar, *Interband resonant transitions in two-dimensional hexagonal lattices: Rabi oscillations, Zener tunnelling, and tunnelling of phase dislocations*, Opt. Express, 16 (2008), pp. 14076–14094.
[29] O. Bahat-Treidel, O. Peleg, M. Segev, and H. Buljan, *Breakdown of Dirac dynamics in honeycomb lattices due to nonlinear interactions*, Phys. Rev. A, 82 (2010), 013830.

[30] P. R. Wallace, *The band theory of graphite*, Phys. Rev., 71 (1947), pp. 622–634.
[31] M. Ablowitz, S. Nixon, and Y. Zhu, *Conical diffraction in honeycomb lattices*, Phys. Rev. A, 79 (2009), 053830.
[32] M. J. Ablowitz and Y. Zhu, *Evolution of Bloch-mode envelopes in two-dimensional generalized honeycomb lattices*, Phys. Rev. A, 82 (2010), 013840.
[33] N. Ashcroft and N. Mermin, *Solid State Physics*, Saunders College, Philadelphia, 1976.
[34] B. Wunsch, F. Guinea, and F. Sols, *Dirac-point engineering and topological phase transitions in honeycomb optical lattices*, New J. Phys., 10 (2008), 103027.
[35] M. J. Ablowitz and Y. Zhu, *Nonlinear diffraction in photonic graphene*, Opt. Lett., 36 (2011), pp. 3762–3764.